Undersea & Hyperbaric Medicine, Vol. 20, No. 1, 1993

Computer simulation of counterlungs

S. P. TOMLINSON, J. LIVESEY, D. G. TILLEY, and I. HIMMENS

Fluid Power Centre, School of Mechanical Engineering, University of Bath, and Defence Research Agency, Maritime Division, ARE Alverstoke, Hants, United Kingdom

Tomlinson SP, Livesey J, Tilley DG, Himmens I. Computer simulation of counterlungs. Undersea & Hyperbaric Med 1993: 20(1):63–73—We have developed a computer model of chest-mounted counterlungs, which accounts for counterlung shape, effective volume, and pressure centroid. The model has been validated and the principles are applicable to other counterlung systems. The highly non-linear and discontinuous behavior of a counterlung is predicted by use of a sophisticated numerical integration method that computes variables such as pressure and volume in the time domain. Three separate stiffness (reciprocal of compliance) terms have been used which contribute to the diver's work of breathing: material elastic stiffness, "gas" stiffness, and "hydrostatic" stiffness. The model provides a significant advance in the understanding of counterlung behavior, allowing the performance of practical equipment to be predicted.

counterlung model, block diagram, numerical integration method, non-linear, gas stiffness, hydrostatic stiffness, computer simulation, Coulomb resistance, pressure centroid, breathing loop, hysteresis, effective area

Rebreathing systems show significant advantages (1:61–68) over demand-regulated, open-circuit scuba and umbilical-fed, open-circuit equipment for underwater exploration: low gas consumption, long endurance, freedom from umbilical restraint, and for military purposes, low acoustic properties. An essential part of rebreather systems is a counterlung, a flexible chest or back-mounted bag that is used to store gas, close to ambient pressure, during the breathing cycle.

The gas flow around a counterlung breathing circuit can be bi-directional (pendulum breathing) with a front-mounted carbon dioxide absorbent canister (Fig. 1A) or unidirectional with the canister back-mounted (Fig. 1B). Both equipments use the semiclosed-circuit, constant-mass-flow principle (1–4) whereby pre-mixed oxygen–nitrogen gases are introduced into the breathing circuit via pressure regulators.

It is important that breathing systems exhibit low pressure losses while supplying sufficient gas to meet diver requirements (5). These requirements can be investigated using computer simulation techniques (5, 6), which provide a means of assessing conceptual designs and improving existing systems while minimizing experimental test work.

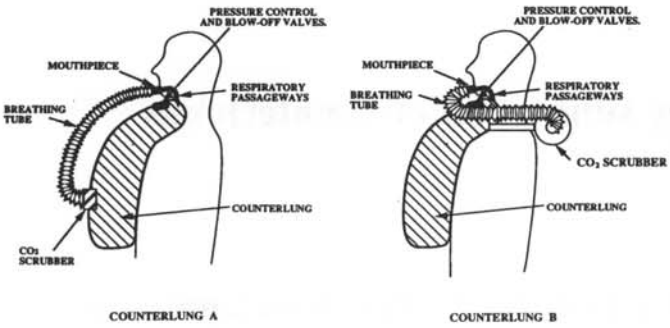

FIG. 1—Counterlungs in semi-closed circuit.

Two factors are important for diver safety and comfort when using rebreathing systems: a) work during breathing and b) hydrostatic pressure imbalance (1). The latter is the differential pressure between the pressure centroid of the counterlung and the diver's lungs under zero flow conditions. The counterlung model is intended to aid the designer in understanding the factors that contribute to breathing work (1, 7, 8) so that this may be minimized. Flow resistive properties of rebreathing systems have also been simulated accurately using the counterlung model (5, 6, 9), which incorporates a true representation of inertial effects necessary at high frequencies.

The operation of a counterlung is extremely complex and depends on shape, material, and construction and diver orientation. We have represented a counterlung as a linear actuator with inertia, spring stiffness, and viscous and Coulomb resistance terms. The latter is a constant friction force and is dependent on material properties. We have also included the effect of changes in pressure centroid and area acted on by pressure forces. The principles used in the model are general and have been applied to three specific chest-mounted counterlungs, referred to as A, B, and C:

1. Counterlung A, a DSSCCD unit made of natural rubber, single-ply cotton reinforced, with material thickness 1.07 mm. This is used in a bi-directional system (Fig. 1*A*).
2. Counterlung B, a SIVA 55 unit made of nylon fabric, polyurethane reinforced, with material thickness 0.97 mm. This is used in a unidirectional system, with similar geometry to counterlung A: lower elastic material stiffness in normal working range (Fig. 1*B*).
3. Counterlung C, a Shark's Sport lightweight prototype unit made of neoprene-coated nylon, with material thickness 0.46 mm. This is used in a bidirectional system, with similar geometry to counterlungs A and B; lowest elastic material stiffness in normal working range (Fig. 1*A*).

We performed considerable validation work with the three counterlungs to justify the assumptions and quantify unknown parameters and relationships used in the model. This was done by immersing the counterlungs in a water-filled tank to determine the variation of counterlung gas pressure with volume, a measure of the diver work of breathing.

METHODS

Counterlung model

Figure 2 is a simplified schematic of a counterlung in the upright position. The three counterlungs are similar in size and shape and a model common to all three units is described. The counterlung face is modeled as a piston of area A moving along an axis, which may be inclined depending on diver orientation. The piston is considered to be a point mass M attached to the diver by a spring and acted on by two pressures: counterlung gas pressure P_c and hydrostatic pressure P_s. For low inflation, the stiffness k of the spring is that due to the "concertinalike" effect of the material as it unfolds. At a certain point in the inflation, the stretching of the material itself becomes significant, resulting in a much larger stiffness. The behavior of the counterlung is affected by the viscous and Coulomb-resistance forces (fdx/dt and F_c) as well as the buoyancy force U and weight component W, which are dependent on diver orientation. The force equation for the counterlung is:

$$M\,d^2x/dt^2 = (P_c - P_s)A + U - W - fdx/dt - kx - F_c \qquad (1)$$

Equation 1 can be integrated successfully to give, respectively, the velocity dx/dt and displacement x of the counterlung face.

Gas flow Q_d (kg/s) takes place into and out of the counterlung control volume V during breathing and the mass flow of gas produced by the motion of the counterlung face is $\rho A dx/dt$ where ρ is the gas density. These flows are used to determine the rate of change of counterlung pressure given by:

$$dP/dt = \frac{nRT}{V}(Q_d - \rho A dx/dt) \qquad (2)$$

where n is the polytropic index, R is the gas constant, and T the temperature of the gas.

Center of pressure (pressure centroid) of a counterlung

The hydrostatic pressure acts at the pressure centroid of a counterlung, which is assumed to contain gas at a uniform pressure. When inflation commences, the

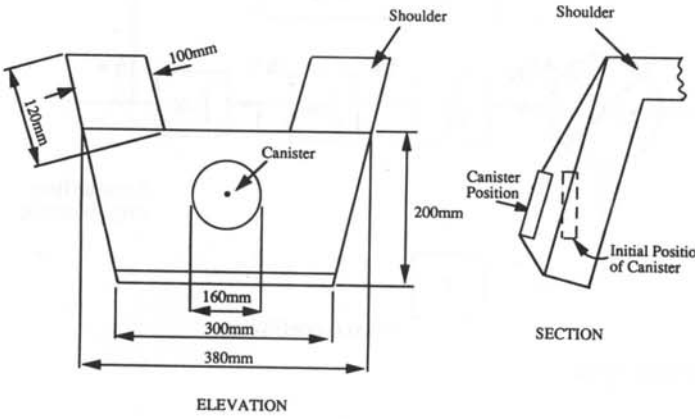

FIG. 2—Counterlung A.

counterlung pressure is equal to the minimum hydrostatic pressure at the top of the counterlung. The pressure centroid x_{po} is the corresponding depth to the top of the counterlung. As air enters, the pressure increases and the shape develops downward under the influence of buoyance, and the distance of the pressure centroid from the top of the counterlung increases. Buoyancy also causes uplift which opposes the filling effect, tending to raise the pressure centroid. These effects have been accounted for by experimental observation and have been substantiated theoretically. The variation in pressure centroid x_p with counterlung displacement x is assumed to be linear and is given by *Eq. 3*.

$$\bar{x}_p = (\bar{x}_{pm} - \bar{x}_{po})\, x/x_m + \bar{x}_{po} \qquad (3)$$

where the subscripts m and o refer to the maximum and zero positions of the counterlung face, respectively, and x_{pm} is orientation dependent.

Effective area acted on by counterlung pressure

Our observations of the inflation and deflation of counterlungs indicate that the effective area acted on by counterlung pressure varies considerably throughout the operational range. The effective area is assumed to increase from a minimum value A_{min} to a maximum value A_{max} and is represented by a cubic polynomial.

$$A = A_{min} + f(x)\,(A_{max} - A_{min}) \qquad (4)$$

where $f(x)$ is given the expression $f(x) = 2z^3 + 3z^2 + 1$ and z is a normalized form of counterlung face displacement x, ranging between zero and unity as x varies between zero and the point at which the frontal area of the counterlung has reached its maximum value.

Net spring effect in a counterlung

Considerable attention has been devoted (10) to identifying the factors that contribute to elastic loads in underwater breathing systems, and the linearized block diagram of the counterlung model (Fig. 3) assists in determining these. The quantities in boxes are gains and the crossed circles indicate that quantities are being summed.

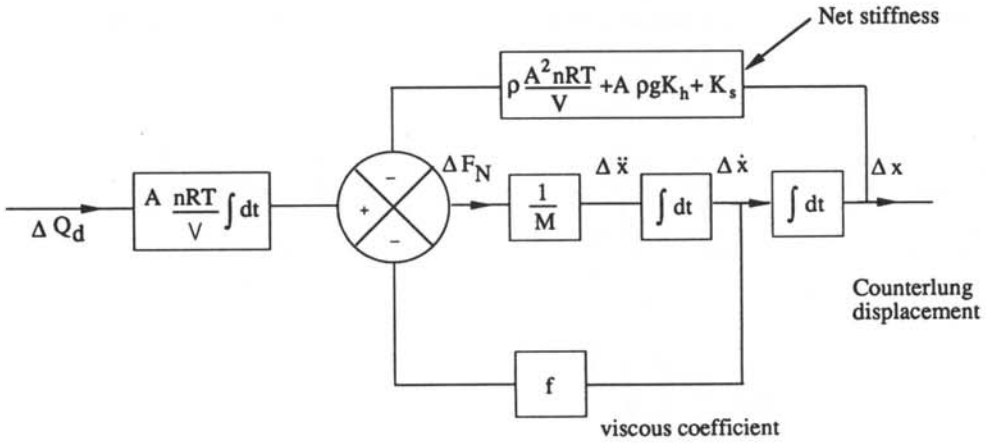

FIG. 3—Block diagram of counterlung model.

In this analysis, small perturbations are considered about a fixed point in the working range of a counterlung. Parameters such as upthrust, weight, and Coulomb resistance disappear from the analysis as they do not contribute to the spring term. The force equation becomes:

$$M\,\delta d^2x/dt^2 = \delta F_n = \delta F - f\delta dx/dt - k\delta x \tag{5}$$

where δ indicates a small perturbation about a mean operating point. The change in applied force δF is given by:

$$\delta F = A\,(\delta P_c - \delta P_s) \tag{6}$$

and the deviation in counterlung pressure δP_c is given by:

$$\delta P_c = \int \frac{nRT}{V}(\delta Q_d - \delta Q_c)\,dt = \int \frac{nRT}{V}(\delta Q_d - \rho A\delta dx/dt)\,dt$$

$$= -\rho\frac{nRTA}{V}\delta x + \int \frac{nRT}{V}\delta Q_d dt \tag{7}$$

The deviation in hydrostatic pressure δP_s is given by:

$$\delta P_s = \rho g k_h A \delta x \tag{8}$$

where k_h is the local gradient $\partial x_p/\partial V$ of the variation in center of pressure x_p with counterlung volume V. Hence

$$\delta F = -\rho\frac{nRTA^2}{V}\delta x - \rho g k_h A^2 \delta x + \int \frac{nRTA}{V}\delta Q_d\,dt \tag{9}$$

Substituting for δF in *Eq. 9*

$$M\delta d^2x/dt^2 = -\{\rho\frac{nRTA^2}{V} + \rho g k_h A^2 + k\}\,\delta x - f\delta dx/dt + \int A\frac{nRT}{V}\delta Q_d\,dt \tag{10}$$

which is represented in Fig. 3. Thus the net stiffness of a counterlung is the displacement-dependent coefficient and comprises the three terms

$$\rho\frac{nRTA^2}{V} + \rho g k_h A^2 + k$$

The "elastic" (recoil) spring effect of the material is the stiffness term k and the "gas" stiffness term is the term $\rho nRTA^2/V$, where A is the frontal area of the counterlung and n is the polytropic index of expansion. The gas stiffness, being dependent on pressure, increases with depth. The "hydrostatic" stiffness due to the variation in pressure centroid with displacement is the term $\rho g k_h A^2$. The summation of these three spring terms determines the gradient $\partial P/\partial Q$ in the pressure-volume diagram, and this together with the viscous and Coulomb resistances determines the diver effort during breathing.

Experimental tests

We performed a series of experimental tests to measure the pressure-volume breathing variations, termed "breathing loops" for the three counterlungs. For each

counterlung, the effects of diver orientation were assessed at the following four extreme positions: (a) upright (vertical); (b) prone (horizontal face down); (c) upside-down (vertical); and (d) supine (horizontal face up).

The counterlung was attached to a mannequin (Fig. 4) mounted in a water-filled reservoir. Air was supplied to the counterlung using a breathing simulator: a reciprocating dual piston device of comparable capacity to the human lungs. Changes in hydrostatic pressure occurred during inhalation and exhalation, and pressure-volume loops were obtained for the three counterlungs in the four orientations.

We measured the rise and fall of water in the tank using a displacement transducer and thus obtained the change in the counterlung volume during inflation and deflation. The volume changes occurred slowly (minimum 15 s) so that measurements were unaffected by inertial effects of the float or water column and the flow resistive pressure loss ΔP was assumed to be zero. A pressure transducer, mounted on the counterlung, was used to measure the corresponding counterlung pressure.

Pressure-volume loops were determined a) from the fully deflated to the fully inflated condition and b) intermediate conditions, more representative of diving. While full inflation and deflation does not generally happen in practice, it enables a full-range theoretical model to be established for use at intermediate conditions. Figure 5 shows the measured pressure-volume loop for counterlung A in the supine position.

Video recordings were taken of the counterlung motion during each test. A graduated scale was placed next to the counterlung to measure the position of the top and bottom of the counterlung during the breathing process. Visual displays were also included on the video film so that the pressure and volume could be determined at any point in the counterlung motion.

RESULTS

Comparison of experimental and simulated behavior

We established a computer model to simulate the counterlung behavior and compared the predictions with experiment results. Figure 6*a* shows the measured pres-

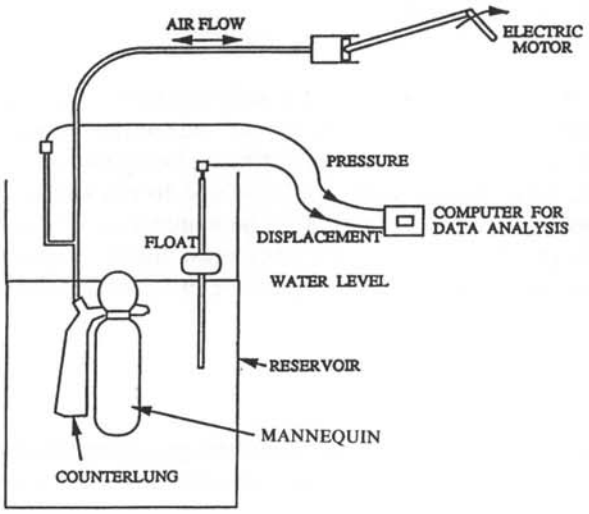

FIG. 4—Experimental rig to determine pressure–volume breathing loop for a counterlung.

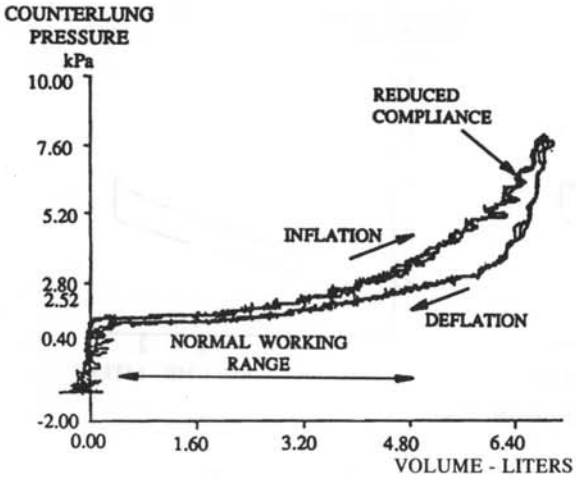

FIG. 5—Counterlung in a supine position.

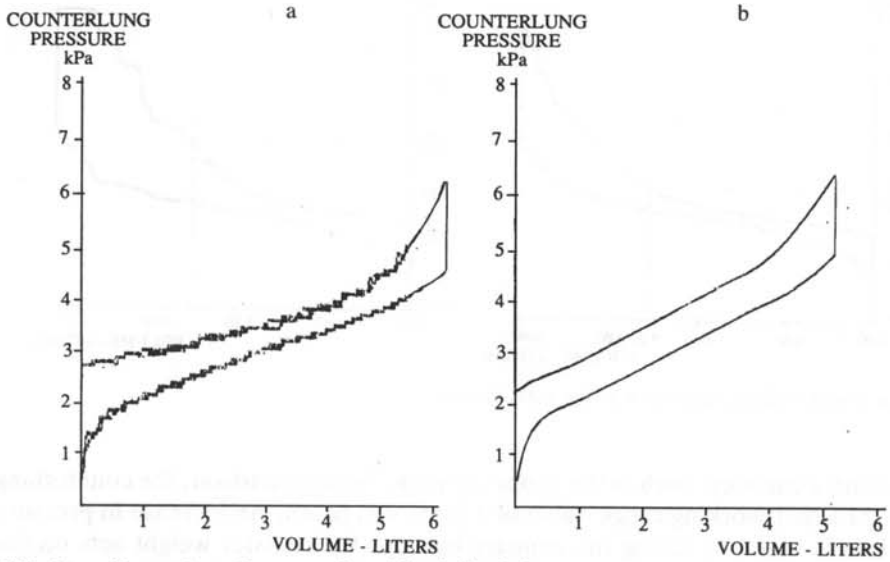

FIG. 6—*a*, Counterlung C measured upright; *b* simulation.

sure-volume loop for counterlung C in the upright condition; Fig. 6*b* shows the corresponding simulation. The simulated pressure in the normal working range increases linearly with volume. This was not born out in practice, and the discrepancy is probably due to the fact that the material stiffness is not constant, as assumed in the simulation. Apart from the differences indicated, there is good agreement between experiment and simulation.

We obtained several intermediate pressure-volume loops at each test condition in the normal working range. Figure 7*a* shows a typical loop for counterlung B in the upright position and Fig. 7*b* shows the corresponding simulation, showing good agreement.

We performed tests to establish the effect of the carbon dioxide canister on the performance of counterlung A. Figure 8*a* shows the loop without a canister and

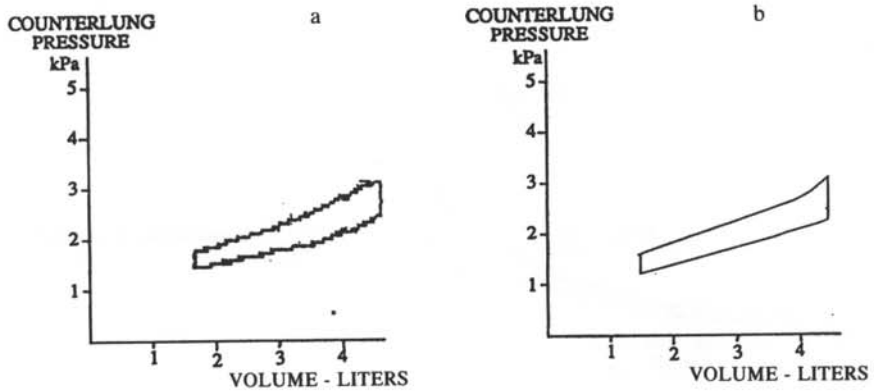

FIG. 7—*a*, Counterlung B measured upright; *b* simulation.

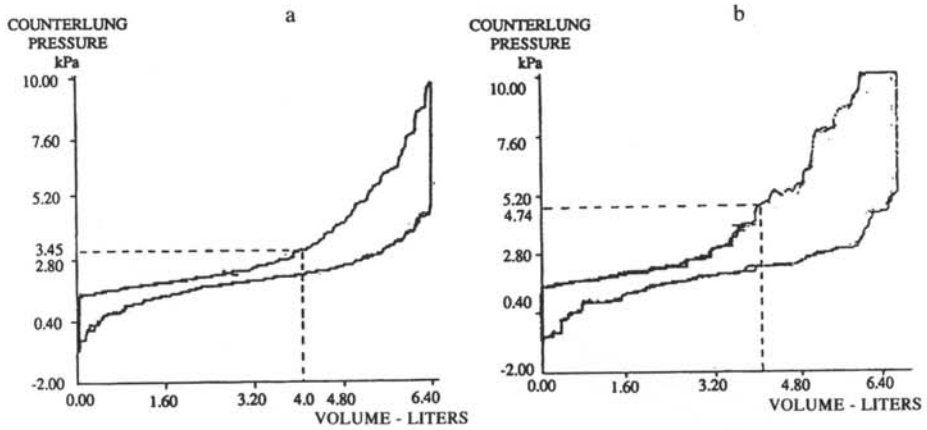

FIG. 8—*a*, Prone without canister; *b* prone with canister.

Fig. 8*b*, with a canister, both in the prone position. For comparison, the counterlung pressure at a mid-working range value of 4 liters was taken. An increase in pressure of 1.29 kPa is noted by fitting the canister because the canister weight acts on the counterlung face. A similar effect was found for the supine position, but for the upright and upside down positions no significant change in counterlung pressure occurred because the weight component is insignificant in these orientations. The model accounts for this effect and predicts similar counterlung pressures in the four orientations.

Magnitude of hysteresis in pressure-volume loop

The hysteresis level is taken as the difference in pressure level between inflation and deflation at a given volume. This is directly related to the Coulomb resistance in the counterlung material. From the experiment, we observed that, for a given orientation, the hysteresis level for counterlung C was considerably lower than either A or B (which were comparable). This is probably due to a lower Coulomb resistance in the counterlung material.

We observed that, for any particular counterlung, the magnitude of the hysteresis is dependent on orientation. A hysteresis level of 1.0 kPa was recorded for counterlung B in the upright position, whereas in the upside-down position, a much lower level of 0.29 kPa was recorded. The corresponding simulations show good correlation with the experimental data. We tested each of the counterlungs and observed that the hysteresis level is much higher when upright than when upside-down, with intermediate levels in the supine and prone positions. We attribute this effect to a difference in the inflation process in the four orientations and that the Coulomb friction level is proportional to the amount of material in motion. In the upright position, the inflation process is approximately uniform over the full face of the counterlung so that the maximum amount of material experiences motion and consequently the Coulomb resistance is highest. In the upside-down position, the inflation process is concentrated more at the top of the counterlung until it is nearly fully developed. Therefore, over a significant range of inflation, a much smaller amount of material experiences motion and the Coulomb resistance will consequently be much smaller.

We observed that the magnitude of the hysteresis level is significantly higher when a counterlung is near to the fully inflated condition because a larger amount of counterlung material is being stretched than during the normal operating range. Consequently, the Coulomb resistance in the counterlung material is much higher.

Comparison of counterlungs

In Table 1 we contrast the measured performance of the three types of counterlung from the viewpoint of working-range stiffness and energy loss in joules per liter. The

Table 1: Comparison of Counterlungs

Type of Counterlung	Position	Gradient $\partial P/\partial Q$ Inflating (1)	Gradient $\partial P/\partial Q$ Inflating (2)	Gradient $\partial P/\partial Q$ Deflating (1)	Gradient $\partial P/\partial Q$ Deflating (2)	Energy Loss, J/liter (1)	Energy Loss, J/liter (2)
A, without canister	upright	0.38	0.36	0.38	0.36	0.22	0.21
	inverted	0.36	0.36	0.36	0.34	0.28	0.27
	supine	0.39	0.34	0.20	0.17	0.28	0.24
	prone	0.30	0.26	0.30	0.26	0.38	0.32
A, with canister	upright	0.50	0.48	0.50	0.48	0.27	0.26
	inverted	0.34	0.33	0.34	0.33	0.23	0.22
	supine	0.58	0.51	0.39	0.35	0.48	0.42
	prone	0.70	0.63	0.46	0.40	1.07	0.94
B	upright	0.34	0.31	0.47	0.41	0.86	0.76
	inverted	0.50	0.50	0.50	0.50	0.21	0.21
	supine	0.42	0.41	0.23	0.22	0.41	0.41
	prone	0.40	0.35	0.75	0.66	1.43	1.23
C	upright	0.27	0.22	0.39	0.35	0.48	0.44
	inverted	(no test possible)					
	supine	0.15	0.14	0.15	0.14	0.14	0.13
	prone	(no test possible)					

Key: (1) = experimental data; (2) = simulation.

energy loss is the area within the pressure-volume loop taken for a fixed end-tidal volume increment. Table 1 also provides a comparison between the measured results and simulation. The elastic work during breathing is directly related to the net spring effect, which is proportional to the gradient $\partial P/\partial Q$ of the pressure-volume curve. Thus, the difference between simulation and experiment in this gradient will reflect the accuracy of the simulation in estimating the elastic work of breathing.

Comparing counterlung types, counterlung C is superior from the viewpoint of stiffness, taken as being proportional to the gradient $\partial P/\partial Q$ in the normal working range. This was expected, because in the working range elastic material stiffness is dependent on the properties of the material fabric. Counterlung C material is very much thinner and lighter than that of either counterlung A or B. The comparison between counterlungs A and B is very much dependent on orientation. From the viewpoint of orientation, there was no simple conclusion and each counterlung showed different characteristics. This is due, in part, to the complicated nature of the inflation and deflation characteristics of the different types of counterlung. As a generalization, the following apply:

1. Coulomb resistance accounts for the magnitude of the hysteresis level and is dependent on how much material in the counterlung is changing shape as pressure is applied. For any counterlung, this is a function of orientation.
2. As the frontal areas of the three types of counterlung are approximately the same, differences in the gradient of the pressure-volume curves between counterlungs are due to the compliance and Coulomb resistance for the counterlung fabric.

The test data provided an insight into the physical behavior of counterlungs, which led to the development of the more representative mathematical model presented, which is intended for use in the assessment of manned diving tests (7).

DISCUSSION

Our general-purpose computer model of a counterlung predicts the behavior of practical equipment to a high degree of accuracy. Extensive practical testing of three types of counterlung has been undertaken to test and refine the model. Although high-frequency data were not available from the experimental tests, we have included the correct inertial terms in the model, which should therefore be accurate for high frequencies. Simulations of a rebreathing system used in diving operations have been performed and compared with measured data to show that the model is valid at depth. The model accounts for the effects of: a) material elastic stiffness, b) hydrostatic stiffness due to the change in pressure centroid with counterlung geometry, c) gas stiffness due to enclosed gas, d) Coulomb resistance in material fabric, e) viscous resistance, f) mass of counterlung, g) shape of counterlung, h) diver orientation, and i) carbon dioxide scrubber.

The model predicts that the weight of the carbon dioxide canister is only significant in the prone and supine positions. This is born out by practical observation of counterlung A and is because the gravitational force acting on the canister has a significant component only when the diver assumes these orientations.

The simulation studies predict that diver orientation significantly affects the work during breathing. This is because the counterlung orientation has a pronounced effect

on the amount of counterlung material acted on by pressure forces. This was found to be least when the diver was upside down. In addition, the simulations have identified a number of significant parameters which contribute to the diver's work of breathing. We recommend the following to minimize this:

1. Ensure that the material elastic stiffness in the working range is minimal by means of a lightweight fabric.
2. Ensure that the change in pressure centroid is minimized during the breathing process.
3. Ensure that the frictional resistance in the counterlung material is minimal.
4. Ensure that the volume of the counterlung is as large as possible.

Manuscript received December 1991; accepted October 1992.

REFERENCES

1. Morrison JB, Reimers SD. Design principles of underwater breathing apparatus. In: Bennett PB, Elliot DH. The physiology of medicine and diving, 3rd ed. San Pedro, CA: Best Publishing, 1982:55–98.
2. Sterk W. Respiratory mechanics of diver and diving apparatus. Drukkerij, Elinkwijk, Holland: University of Utrecht. 1973. Thesis.
3. Morrison JB. Evaluation of alternative gas delivery systems for semi-closed circuit underwater breathing apparatus. In: Lundgren CEG, Warkander DE, eds. Physiological and human engineering aspects of underwater breathing apparatus. Bethesda, MD: Undersea and Hyperbaric Medical Society, 1989:139–152.
4. Fullerton and Sherwood. OM-1 gas mixing circuit. Preliminary report to DCIEM. Ontario. Canada: Fullerton and Sherwood Engineering Ltd, 1986.
5. Tilley DG, Livesey J, Tomlinson SP, Himmens IA. An approach to the modelling of underwater breathing apparatus. In: Lundgren CEG, Warkander DE, eds. Physiological and human engineering aspects of underwater breathing apparatus. Bethesda, MD: Undersea and Hyperbaric Medical Society, 1989:125–137.
6. Tilley DG, Livesey J, Tomlinson SP. Computer simulation of a semi-closed breathing system. 1991; J Systems Control Eng I Mech E, October 1991.
7. Sarhan NAS, Leaning MS, Saunders KB, Carson, ER. Development of a complex model: breathing and its control in man. Biomed Meas Infor Contr 1987–88; 2(2).
8. O'Neill WJ. A study of the breathing hydrostatics of various bag-type diving apparatuses and description of the two valve Toroidal and Abalone back-mounted design. In: Equipment for the working diver. Washington, DC: Marine Technology Society, 183–211.
9. Tomlinson SP, Tilley DG. The digital simulation of underwater breathing equipments. Final contract report. Report no 1023, Fluid Power Centre, School of Mechanical Engineering, University of Bath, UK, April 1990.
10. Joye DD, Clarke JR, Carlson NA, Flynn ET. Formal descriptions of elastic loads encountered in the use of underwater breathing systems. In: Lundgren CEG, Warkander DE, eds. Physiological and human engineering aspects of underwater breathing apparatus. Bethesda, MD: Undersea and Hyperbaric Medical Society, 1989:59–76.